ACS APPLIED NANO MATERIALS

www.acsanm.org Article

Antibody-Conjugated Barium Titanate Nanoparticles for Cell-Specific Targeting

Tomas Jordan, Mikaela A. O'Brien, Catalina-Paula Spatarelu, and Geoffrey P. Luke*

Cite This: https://dx.doi.org/10.1021/acsanm.0c00019 Read Online

ACCESS | Metrics & More | Article Recommendations | Supporting Information

ABSTRACT: Barium titanate nanoparticles (BTNPs) are gaining popularity in biomedical research because of their piezoelectricity, nonlinear optical properties, and high biocompatibility. However, the potential of BTNPs is limited by the ability to create stable nanoparticle dispersions in water and physiological media. In this work, we report a method of surface modification of BTNPs based on surface hydroxylation followed by covalent attachment of hydrophilic poly(ethylene glycol) (PEG) polymers. This polymer coating allows for additional modifications such as fluorescent labeling, surface charge tuning, or directional conjugation of IgG antibodies. We demonstrate the conjugation of anti-EGFR antibodies to the BTNP surface and show efficient molecular targeting of the nanoparticles to A431 cells. Overall, the reported modifications aim to expand the BTNP applications in molecular imaging, cancer therapy, or noninvasive neurostimulation.

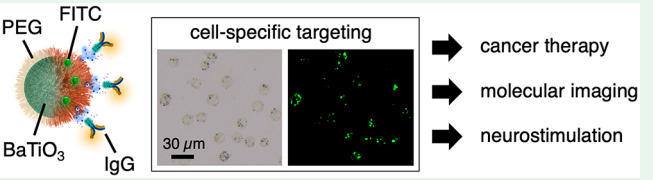

KEYWORDS: *barium titanate nanoparticles, surface hydroxylation, poly(ethylene glycol), fluorescence, antibody conjugation, molecular targeting*

INTRODUCTION

Barium titanate is a ceramic material with perovskite structure. It is characterized by a high dielectric constant and excellent ferroelectric and piezoelectric properties.[1] These characteristics make it attractive for use in capacitors and other electronic devices. Recently, there has been growing interest in barium titanate in nanoparticle form. Although barium titanate nanoparticles (BTNPs) are widely utilized in the microelectronics industry, recent research indicates that BTNPs have a strong potential for biomedical use thanks to their high biocompatibility.[2−6] They also demonstrate a distinct set of mechanical, electrical, and optical properties which make them uniquely suited for a variety of applications. In particular, BTNPs are capable of exhibiting nanoscale piezoelectricity and producing second-harmonic optical responses. These two starkly different properties have led to wide-scale investigations into their application in biotechnology.

The therapeutic potential of BTNPs stems from the high piezoelectric coefficients of barium titanate in tetragonal crystalline phase.[7] Nanoparticle piezoelectricity is attractive for applications in tissue engineering as the piezoelectric effect promotes bone growth or nervous tissue repair.[8,9] The addition of hypergravity to piezoelectric nanoparticles further aids bone regeneration by enhancing differentiation of mesenchymal stem cells into osteoblasts.[10] The piezoelectric effect can also be exploited to enable wireless electrical stimulation of cells; when BTNPs are stimulated noninvasively with ultrasound, they generate electric charges on their surfaces. Thanks to this phenomenon, ultrasound-stimulated BTNPs bound to membranes can induce calcium and sodium fluxes in neuron-like cells and reversibly increase the electrical activity of in vitro neural networks.[11,12] Additionally, the newest research suggests that electrical stimulation resulting from the ultrasound-induced piezoelectric effect may be capable of inhibiting the proliferation of cancer cells. Chronic ultrasound stimulation of BTNPs possibly interferes with cells' calcium homeostasis and may cause reorganization of the mitotic spindle, leading to antiproliferative effects in HER-2 positive breast cancer cells and glioblastoma cells.[13,14] Furthermore, BTNPs coated with gold enable photothermal therapy of cancerous lesions, and polymeric coatings can facilitate gene or drug delivery. Thus, BTNPs have a strong potential to be applied as a multifunctional anticancer agent.[15]

Next to applications in cancer therapy and neurostimulation, BTNPs also act as a contrast agent for medical imaging. The nanoparticles have the ability to generate second harmonic optical signal due to their noncentrosymmetric structure. Although the generation of the second harmonic signal is less efficient than fluorescence, the effect offers numerous benefits over conventional fluorescence imaging. While fluorophores saturate, photobleach, and fluctuate in emission intensity, the signal from second harmonic generating crystals is stable and does not saturate with increasing intensity of illumination.[16]

Received: January 3, 2020
Accepted: March 5, 2020
Published: March 5, 2020

Scheme 1. Surface Modifications of Barium Titanate Nanoparticles

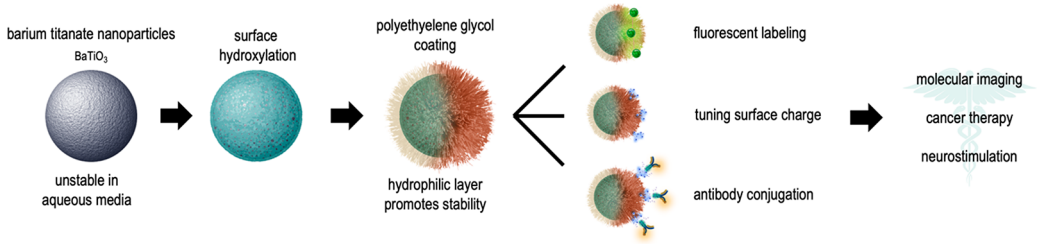

Furthermore, the second harmonic generation (SHG) signal has exquisite photostability and can be sensed with minimal background signal, eliminating issues linked to tissue autofluorescence. Other advantages of SHG include a narrow emission bandwidth, a coherent signal, flexible excitation wavelengths, and femtosecond-scale response times. BTNPs have successfully been used in a wide variety of SHG imaging applications as an alternative to fluorescence imaging. In vivo examples include imaging of zebrafish embryos or imaging BTNPs through mouse tail tissue.[17,18] When combined with super-resolution techniques, BTNPs can be used to quantify mRNA with single copy sensitivity and resolution on the order of tens of nanometers.[19] This mRNA quantification technique has the potential to outperform established methods such as fluorescence in situ hybridization or quantitative PCR. Volumetric SHG imaging has also been reported using a harmonic holographic microscope.[20] Combining the therapeutic effects and SHG potential, BTNPs could be used to deliver piezoelectric stimuli to cells while simultaneously imaging where the stimuli are being applied.

While typical BTNP synthesis methods such as solid-state reactions or sol−gel methods involve extreme environments and high temperatures, recent publications report soft chemistry synthesis methods enabling the expansion of BTNP research.[2,21−25] Regardless of the synthesis method, the applications of BTNPs are challenged by the ability to create stable dispersions in water as the nanoparticles have minimal stability and quickly aggregate in aqueous media with pH values lower than 12.[26] The literature contains reports of numerous techniques of BTNP stabilization by coating the surface with a polymer layer. Early studies utilized poly(L-lysine) to wrap the nanoparticle surface to create BTNP dispersions stable for multiple days. However, the polymer was found to induce cytotoxic effects.[27] Stable BTNP dispersions without cytotoxic effects have since been achieved using other polymers such as glycol chitosan or polyethylenimine.[5,28] These polymeric wrapping techniques rely on nonspecific adsorption and noncovalent binding, which could result in decreased stability in biological environments. As an effort to combat this shortcoming, cyclodextrin (CD)-stabilized BTNPs were prepared by first hydroxylating the nanoparticle surface and then covalently attaching CD molecules, leading to stable and noncytotoxic dispersions of BTNPs.[29] However, BTNP stabilization through covalent binding of a hydrophilic polymer such as poly(ethylene glycol) (widely utilized in drug delivery for its superior ability to increase the solubility of hydrophobic substances) has not been reported.

Molecular targeting via conjugating antibodies to the surface of nanoparticles can enable specific delivery of therapeutic agents or imaging of specific biological processes.[30] Some early steps toward molecular targeting of BTNPs have been reported. The first method relies on reduction of the disulfide bonds in the antibody hinge region to create fragments with exposed free thiol groups.[31] The reduced antibody fragments can then be conjugated to nanoparticles functionalized with maleimide groups. While this technique succeeds in targeting BTNPs to HeLa cells, it includes modifications of the functional binding regions, which could impact specificity. The second method is based on reacting biotin-functionalized BTNPs with streptavidin−antibody conjugates. This specific example uses an antibody against the transferrin receptor to target the nanoparticles to glioblastoma cells.[14] However, the chemistry is dependent on the availability of antibodies with conjugated streptavidin. Furthermore, the antibodies are bound nondirectionally which decreases the probability of the binding regions having the appropriate orientation.

In this work we report a new method for preparing dispersions of BTNPs which is based on covalent attachment of poly(ethylene glycol) (PEG) molecules to the nanoparticle surface (as illustrated in Scheme 1). The PEG polymers are hydrophilic leading to improved nanoparticle stability. Furthermore, PEG has a proven track record of biocompatibility and is readily functionalizable.[32,33] Our chemistry is based on hydroxylating the BTNP surface via thermal decomposition of hydrogen peroxide.[34] The creation of hydroxyl groups allows binding of readily available silane-functionalized PEG polymers.[35] Furthermore, this technique gives rise to the use of heterobifunctionalized PEG molecules enabling tuning of the surface charge, manufacturing of fluorescent BTNPs, and generation of free functional groups for further surface modifications. We harness these free functional groups to covalently bind targeting antibodies without antibody reduction or streptavidin labeling, leading to directional conjugation of intact antibodies. The chemistry is flexible and can be applied to any IgG antibody with a glycosylated Fc region. It is based on the derivation of free aldehyde groups on the Fc region and the use of a heterobifunctional cross-linker to create covalent bonds between the antibody and the functionalized PEG molecules on the nanoparticle surface. This versatile surface modification approach aims to expand the biomedical BTNP applications by preparing stable nanoparticle dispersions in physiological media and allowing the BTNPs to be targeted to specific cells of interest for the purposes of imaging, cancer therapy, or neurostimulation.

EXPERIMENTAL SECTION

Materials. Barium titanate nanoparticles ($BaTiO_3$, 300 nm) in tetragonal phase were purchased from Nanostructured & Amorphous Materials, Inc. Silane-functionalized poly(ethylene glycol) (10 kDa mPEG-silane) was obtained from Creative PEGWorks while heterobifunctionalized polymers (5 kDa silane-PEG-SH, 2 kDa silane-PEG-COOH, 2 kDa silane-PEG-NH_2, and 5 kDa silane-PEG-FITC) were purchased from Nanocs Inc. The polydispersity index of

https://dx.doi.org/10.1021/acsanm.0c00019
ACS Appl. Nano Mater. XXXX, XXX, XXX−XXX

all used polymers was <1.1 as reported by the manufacturer. Fluorescent dyes (sulfocyanine3 maleimide, sulfocyanine5 NHS ester) were acquired from Lumiprobe Corporation. EGFR monoclonal antibody (clone 225), fluorescent labeling kit (Alexa Fluor 555), and cross-linker (EMCH) were purchased from ThermoFisher Scientific. Reagents for the conjugation reaction included sodium phosphate dibasic, sodium periodate, HEPES, and 1x phosphate buffered saline (PBS) which were all obtained from Millipore Sigma. All of the used products with their corresponding catalog numbers are listed in Table S1 of the Supporting Information.

Surface Hydroxylation. The powdered BTNPs (200 mg) were mixed with 30% hydrogen peroxide (200 mL) in a 500 mL Erlenmeyer flask covered with parafilm. The mixture was placed on a hot plate and brought to 85 °C while stirring. The reaction time was varied from 30 min to 8 h. Afterward, the nanoparticles were centrifuge washed three times with 95% ethanol (4500 RCF for 10 min) and then suspended in 20 mL of 95% ethanol to yield a 10 mg/mL stock solution. To investigate the effects of hydroxylation and varying reaction times, Fourier-transform infrared spectroscopy (FTIR) was utilized. Hydroxylated nanoparticles were dried into a powder and analyzed with a Jasco 6200 spectrometer. FTIR spectra were obtained using an attenuated total reflectance (ATR) accessory.

BTNP Stabilization through Poly(ethylene glycol) (PEG) Coating. Silane-functionalized PEG polymers were attached to the BTNPs covalently through binding between silanes and hydroxyl groups on the nanoparticle surface.[35] First, 20 mg of mPEG-silane (MW 10 kDa) powder was dissolved in 9 mL of 95% ethanol (with catalytic 5% of DI water). This reaction mixture was combined with 1 mL of the hydroxylated nanoparticle solution (10 mg/mL), and the product was sonicated with a tip sonicator (Qsonica) for 2 h (amplitude 25, 3 s ON, 25 s OFF). The solution was covered and left to react overnight, and then unbound PEG molecules were eliminated by three centrifuge washes with DI water (4500 RCF for 8 min). The pellet was resuspended in 10 mL of DI water, yielding 1 mg/mL solution of PEG-coated nanoparticles. To verify the successful binding of PEG molecules, mPEG-silane was replaced with 5 kDa silane-PEG-FITC, and green fluorescent signals were analyzed with fluorescence microscopy (Leica Dmi8 with DFC7000T camera). We segmented wide-field-of-view fluorescent images in Matlab using the Image Processing Toolbox to isolate regions of nanoparticles. Pixel values were summed over these regions, and values of fluorescence per nanoparticle were calculated for a large number of BTNPs ($n > 1000$). For further quantification, PEG-FITC binding was analyzed by using a spectrofluorometer (Horiba FluoroMax-4). The calibration curve for the FITC concentration was established to quantify the amount of silane-PEG-FITC bound to the BTNPs. From the calculated number of polymers bound and the surface area of a single BTNP (provided by the manufacturer), the spacing between individual PEG molecules was calculated.

Functional Groups, Fluorescent Labeling, and Tuning the Surface Charge. Coating of BTNPs with bifunctional PEG molecules enabled additional modifications by creating free functional groups on the surface. To facilitate reactions with gold or to conjugate antibodies, BTNPs were functionalized with thiol groups by adding a 5−20% portion of 10 kDa silane-PEG-SH to the PEG reaction mixture. Green fluorescent BTNPs were created by adding a 10−20% portion of 5 kDa silane-PEG-FITC. Some biomedical applications may require other fluorescent colors, but silane-PEG polymers functionalized with different fluorophores are not readily available. To address this gap in the market, orange fluorescent PEG was created by mixing silane-PEG-SH with sulfocyanine3 maleimide (2.5× molar excess of the fluorophore). Similarly, red fluorescent PEG was prepared by reacting sulfocyanine5 NHS ester with silane-PEG-NH_2. Successful fluorescent labeling was verified by fluorescent microscopy. Another variable relevant to preparing nanoparticle dispersions for biomedical applications is the surface charge since it can affect the binding of nanoparticles to cell membranes and mediate cellular uptake.[28] To shift the nanoparticle charge to more negative values, a 10−50% portion of silane-PEG-COOH was added to the PEG reaction mixture. For more positively charged particles, 10−50% of silane-PEG-NH_2 was used. The effects on the surface charge were investigated by taking ζ-potential measurements using the Malvern ZetaSizer Nano instrument. The exact PEG amounts and the proportions of mPEG-silane to bifunctionalized PEG molecules are listed in Table S2.

Characterization. The size and morphology of the BTNPs were investigated by transmission electron microscopy (TEM). The nanoparticles were deposited on hexagonal copper grids (300 mesh) with carbon film and imaged with FEI Tecnai F20ST (field emission gun operated at 200 kV accelerating voltage). We obtained the size distribution of the BTNPs from TEM micrographs by measuring the diameter of a large number of nanoparticles ($n = 130$) using ImageJ. To identify the nanoparticle crystalline phase, X-ray powder diffraction was utilized. BTNPs in powdered form were deposited on a glass plate and analyzed by using a Siemens D5000 XRD system. To illustrate the piezoelectric properties of individual nanoparticles, piezoresponse force microscopy (PFM) was employed. BTNPs conjugated to thiol-functionalized PEG were deposited on a gold-plated microscope coverslip. Contact mode scanning was performed by using the AIST-NT SmartSPM 1000 instrument while applying 425 kHz AC voltage between the cantilever tip and the substrate to induce the converse piezoelectric effect. The lock-in amplifier built into the instrument was then used to obtain the magnitude and phase of the converse piezoelectric effect.

Directional Antibody Conjugation. The epidermal growth factor receptor (EGFR) antibody was first filtered through a 30 kDa MWCO centrifuge filter (3600 rpm for 15 min) to achieve 1 mg/mL concentration and then fluorescently stained with an Alexa Fluor 555 antibody labeling kit following the standard protocol (provided by ThermoFisher Scientific). To eliminate excess dye, the antibody solution was filtered with the 30 kDa centrifuge filter two times (3600 rpm for 15 min), replacing the original buffer with 1.3 mL of 100 mM Na_2HPO_4. The protocol for derivation of aldehyde groups on the Fc region was adapted from previous work with noble metal nanoparticles.[36,37] The antibody solution was mixed with 80 μL of freshly prepared 100 mM $NaIO_4$, leading to oxidation of the glycosyl groups. After 30 min of shaking in the dark, 500 μL of PBS was added to the mixture, and the presence of aldehydes was confirmed by a Purpald test. The solution was then filtered with a 30 kDa centrifuge filter again (2000 RCF for 10 min); the antibodies were suspended in 400 μL of 40 mM HEPES and stored at 4 °C as a stock solution.

To conjugate the antibodies to the surface of thiol-functionalized BTNPs, a heterobifunctional cross-linker *N*-ε-maleimidocaproic acid hydrazide (EMCH) was used. First, 30 μL of 10 mM solution of EMCH in DMSO was mixed with 1 mL of a coupling buffer (0.1 M sodium phosphate, 0.15 M NaCl, pH 7.2) to create a reaction mixture. Then 30 μL of the antibody stock solution was added and incubated for 2 h in the dark at room temperature. To eliminate excess cross-linker, the mixture was filtered with a 30 kDa centrifuge filter three times (2000 RCF for 10 min) and resuspended in 100 μL of the coupling buffer. Then, 50 μL of this antibody−EMCH solution was mixed with 1 mL of the coupling buffer and 600 μL of 1 mg/mL thiol-functionalized BTNPs. The mixture was incubated for an hour and then washed five times via centrifugation (4000 rpm for 4 min) to remove the unbound antibody. The final BTNP−antibody conjugate solution was resuspended in 600 μL of PBS.

Molecular Targeting to A431 Cell Line. A431 cells (ATCC) were adopted as an in vitro model of human epidermoid carcinoma. This cell line greatly overexpresses EGFR on the surface which enables molecular targeting via the anti-EGFR antibody. The cells were cultured in T-75 flasks by using Dulbecco's Modified Eagle's Medium (DMEM) supplemented with 10% fetal bovine serum and 1% penicillin. Before the targeting experiments, the cells were suspended in 2 mL of DMEM. Then, 200 μL of the cell solution was treated with 70 μL of 200 μg/mL solution of green-fluorescent BTNPs with conjugated anti-EGFR antibodies and incubated for 2 h at 36 °C. Three control experiments were carried out. First, to investigate the levels of nonspecific binding, the cells were incubated with BTNPs without conjugated antibodies. Second, to block the specific receptors and, thus, inhibit any EGFR-mediated BTNP

https://dx.doi.org/10.1021/acsanm.0c00019
ACS Appl. Nano Mater. XXXX, XXX, XXX−XXX

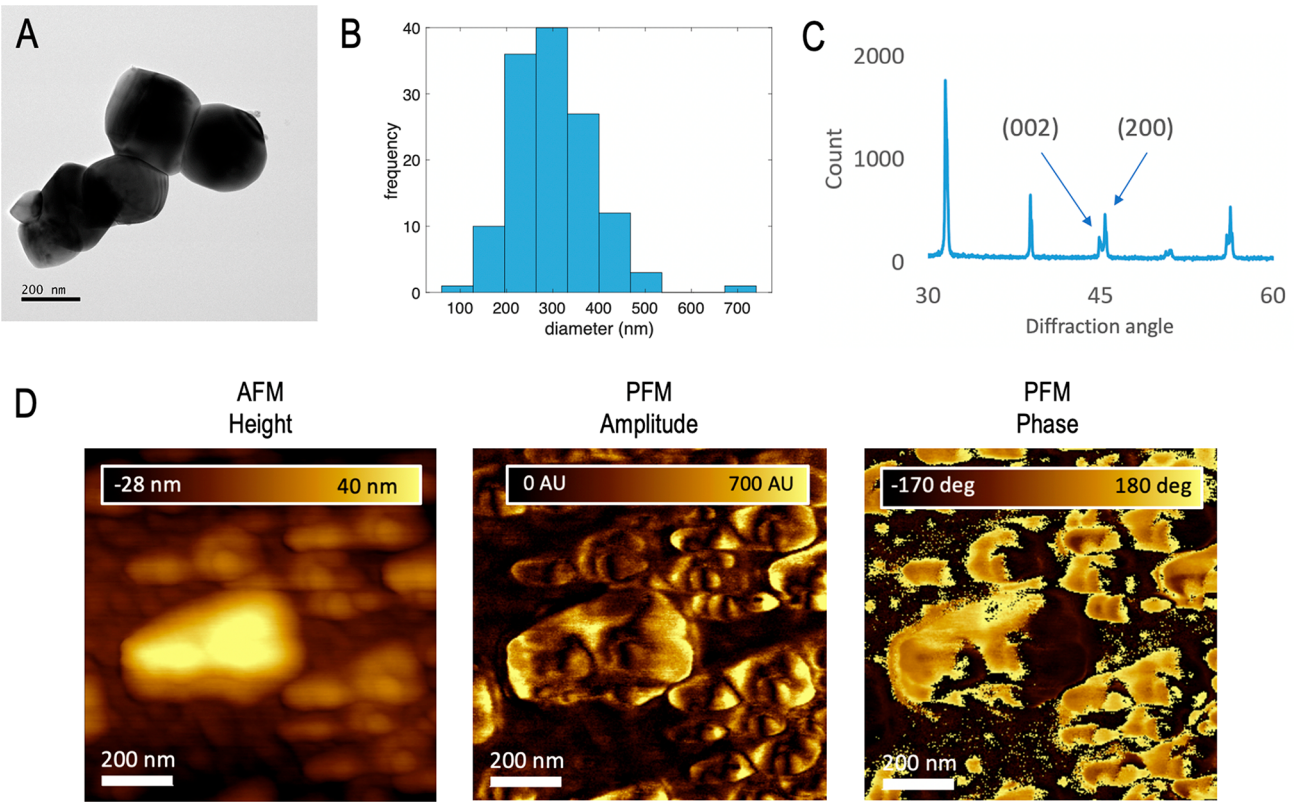

Figure 1. (A) TEM micrograph showing BTNP size and morphology. (B) BTNP size distribution as quantified from TEM. (C) XRD measurement confirming tetragonal phase. (D) Atomic force microscopy (AFM) showing topology of the sample (left) compared with corresponding piezoresponse magnitude and phase (center and right).

binding, the BTNP−EGFR conjugates were incubated with the cells in the presence of free-floating anti-EGFR IgG. Third, an additional control experiment was carried at 4 °C to inhibit cell endocytosis. To clear the unbound BTNPs after a 2 h incubation, the solution was filtered through a 5 μm centrifuge filter (Millipore Sigma UFC30SV00). The cells were then resuspended in 100 μL of PBS and imaged under a microscope (Leica Dmi8) at a 20× magnification to collect bright field and green fluorescence images. To quantify the BTNP fluorescence, we segmented bright field images in Matlab using the Image Processing Toolbox (MathWorks) to isolate individual cells. Regions with corresponding coordinates were then isolated from the green fluorescent images, and pixel values were summed to obtain BTNP fluorescence per cell. To analyze the differences between the targeted BTNPs and the control conditions, images of $n = 60$ cells for each group were quantified, and the distributions were plotted in a box plot. The statistical significance of the results was determined by using the Mann−Whitney U-test.

RESULTS AND DISCUSSION

Nanoparticle Characterization. We imaged commercially available BTNPs with a transmission electron microscope to investigate their size and morphology. Figure 1A depicts a cluster of BTNPs, illustrating their approximately spherical shape. From the micrographs, we obtained the size distribution with a mean of 302.3 nm and standard deviation of 88.2 nm (Figure 1B). Next we investigated the nanoparticle crystal structure using X-ray powder diffraction (XRD). The exact relationship between the BTNP size and their crystal structure is not understood. However, it is reported that below 100 nm the BTNPs transition into cubic phase, leading to a decrease in the d_{33} constant and loss of piezoelectric properties.[38] Our results show separation in (002) and (200) XRD peaks appearing as a double peak near the diffraction angle of 45°, which confirms that the crystal structure is tetragonal (Figure 1C). To demonstrate the nanoparticle piezoelectricity (which is critical for therapeutic benefits), we investigated the piezoelectric effect on a single nanoparticle level. Contact mode piezoresponse force microscopy (PFM) was employed to scan a sample of BTNPs bound to a conductive gold substrate. Upon application of 10 V AC voltage (driven at 425 kHz) between the tip and the substrate, we observed the converse piezoelectric effect. The lateral magnitude and phase of the piezoelectric effect were retrieved using a lock-in amplifier, and they are displayed in Figure 1D. The variations present in the PFM signal can be explained by the fact that the nanoparticles consist of multiple stochastically oriented ferroelectric domains.

Surface Hydroxylation. Studies have shown that thermal treatment of H_2O_2 in aqueous solutions of ceramic oxides leads to decomposition of H_2O_2 and hydroxylation of the ceramic oxide surface.[39,40] This phenomenon has been demonstrated specifically with BTNPs where free hydroxyl groups were derived by refluxing the nanoparticles in aqueous solution of H_2O_2 at 106 °C for 4 h.[34] However, this high temperature approaches the Curie temperature of barium titanate where the material undergoes a transition between its ferroelectric and nonferroelectric structures.[41] Thus, hydroxylating at high temperatures could limit the piezoelectric properties and hinder the therapeutic potential. We investigated BTNP hydroxylation at 85 °C while varying the reaction time from 30 min to 8 h. The levels of hydroxyl group coverage were monitored by FTIR where O−H bond stretching is manifested as a peak in the 3900−2800 cm^{-1} spectral region.[42] As apparent from a close-up view of this region (Figure 2A), the

https://dx.doi.org/10.1021/acsanm.0c00019
ACS Appl. Nano Mater. XXXX, XXX, XXX−XXX

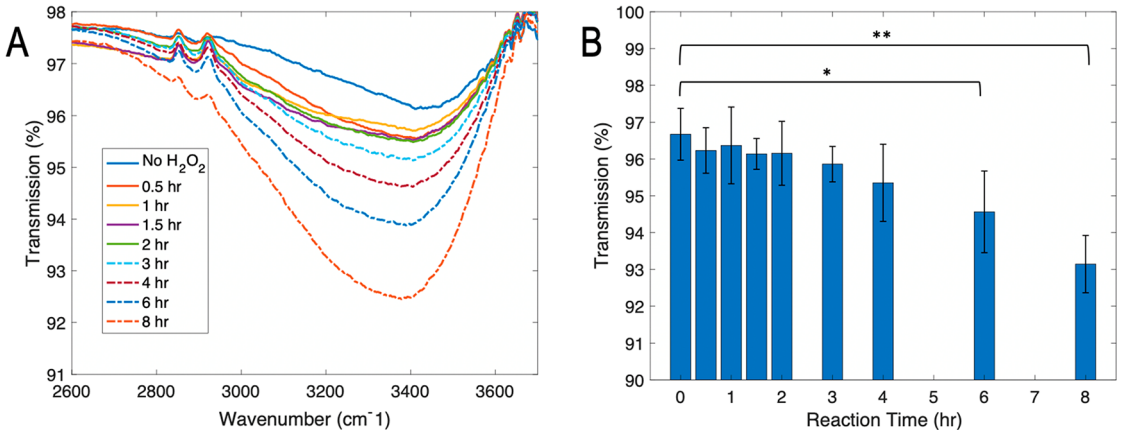

Figure 2. (A) ATR-FTIR spectra of unmodified BTNPs vs hydroxylation times ranging from 30 min to 8 h. This close-up view depicts the peak which corresponds to O−H bond stretching. (B) FTIR peak values averaged over three trials showing increasing absorption with longer hydroxylation times (*p = 0.049, **p = 0.004).

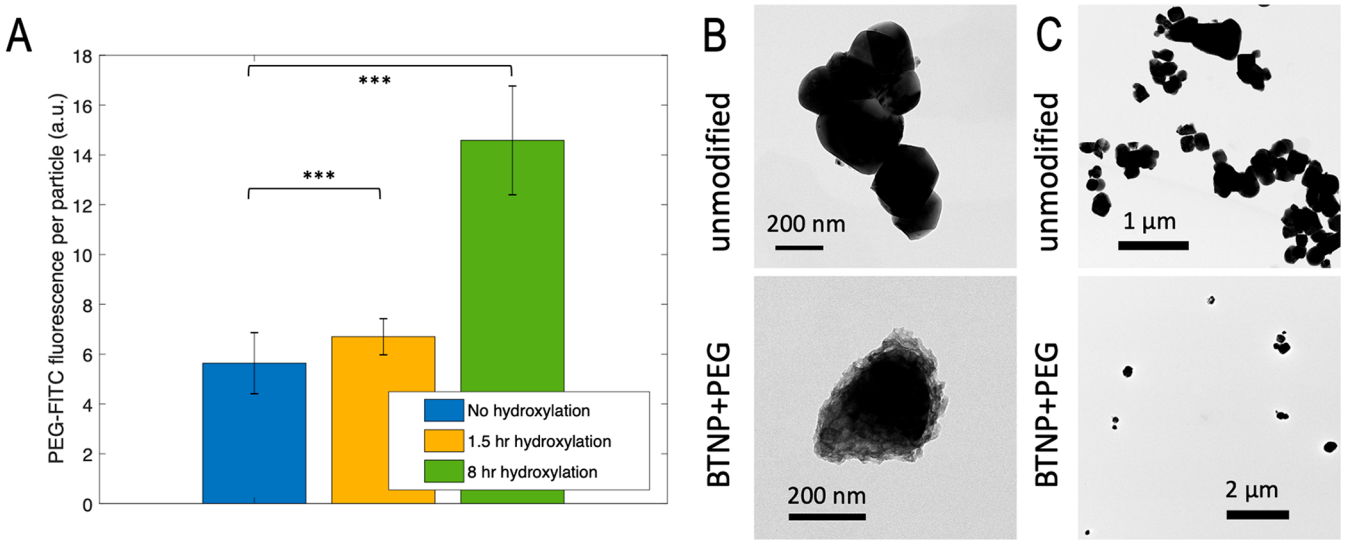

Figure 3. (A) Fluorescence of PEG-FITC bound to BTNPs under different hydroxylation conditions. Hydroxylated nanoparticles had a statistically significant increase in FITC fluorescence with p-values lower than 0.001 (n = 1597). (B) Close-up TEM images comparing the BTNPs before and after PEGylation of the surface. The polymer layer can be seen covering the surface of the modified nanoparticle. (C) The unmodified BTNPs are not stable in aqueous media and form large aggregates. However, upon stabilization with PEG, the BTNPs are well dispersed in water as apparent from the TEM images.

magnitude of the peak corresponding to the O−H bond stretching grows with increasing hydroxylation time, suggesting denser hydroxyl coverage of the nanoparticle surface. Statistical significance was determined based on n = 3 trials by using an unpaired two-tailed Student's t test comparing the different time points to unmodified nanoparticles. For the 6 h hydroxylation time point, the difference compared to unmodified BTNPs is statistically significant with a p-value <0.05. In the case of the 8 h hydroxylation, the result is statistically significant with $p < 0.01$ (Figure 2B).

Poly(ethylene glycol) (PEG) Surface Coating. We exploited the derived free hydroxyl groups to coat the nanoparticle surface with PEG molecules via the covalent binding between silane and hydroxyl. Three conditions were investigated: PEGylation of unmodified BTNPs, PEGylation of BTNPs hydroxylated for 1.5 h, and PEGylation of BTNPs hydroxylated for 8 h. Silane- and FITC-bifunctionalized PEG chains were reacted with the BTNPs in ethanol with a catalytic amount of water under thorough sonication with a tip sonicator. Fluorescence microscopy confirmed the presence of a fluorescent PEG layer. Furthermore, there was an increase in fluorescent signal for nanoparticles that had been hydroxylated, and longer hydroxylation led to brighter signals (Figure 3A). While the mean fluorescence per nanoparticle was 5.6 ± 1.5 au in the unmodified BTNP case, the value rose to 6.9 ± 0.55 au in the 1.5 h hydroxylation condition and 15 ± 4.8 au in the 8 h hydroxylation condition (n = 1597). The presence of bound PEG molecules on the unmodified nanoparticles and only a small increase for the 1.5 h hydroxylation condition can be explained by the fact that even unmodified nanoparticles have a small portion of their surface covered with hydroxyl groups.[43] However, our results support the claim that a longer hydroxylation time leads to denser hydroxyl group coverage as more free hydroxyls provide more available binding sites for the PEG polymers. The statistical significance of these results was assessed by a two-tailed Student's t test. Both hydroxylation conditions were

https://dx.doi.org/10.1021/acsanm.0c00019
ACS Appl. Nano Mater. XXXX, XXX, XXX−XXX

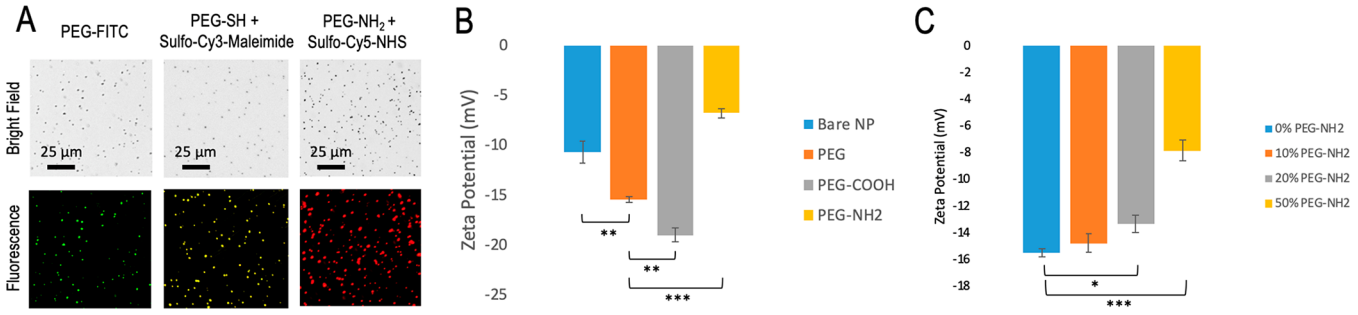

Figure 4. (A) Different colors of fluorescent BTNPs were prepared to be used with standard fluorescent light sources (488, 532, and 633 nm). (B) The surface charge of the BTNPs can be adjusted by incorporating positively or negatively charged functional PEG molecules. While PEG-COOH makes the BTNP surface more negative, PEG-NH_2 shifts the ζ-potential to more positive values. (C) The change in the surface charge induced by the incorporation of charged PEG in the surface coating can be adjusted by varying the proportion of the bifunctionalized charged PEG to the monofunctionalized PEG with no charged groups. Here, increasing the proportion of PEG-NH_2 to PEG in the surface coat leads to an adjustable increase in the ζ-potential.

found to be significantly different from the non-hydroxylated nanoparticles with p-values smaller than 0.001.

To quantify the amount of PEG bound to the BTNP surface, we analyzed the samples using a spectrofluorometer upon establishing a calibration curve for the concentration of silane-PEG-FITC. The non-hydroxylated BTNP sample contained approximately 17.7×10^3 PEG chains per nanoparticle, which corresponds to 4.50 nm spacing between individual PEG grafts. On the other hand, the 8 h hydroxylation BTNP sample contained 49.3×10^3 PEG chains per nanoparticle, averaging 2.70 nm spacing between polymers—a coverage more than twice as dense. These calculations are described in detail in Figure S1, which also displays spectrofluorometer data.

To offer visual evidence of the presence of the PEG layer, we imaged the nanoparticles under TEM. Figure 3B shows a comparison between the unmodified, as-purchased BTNPs and a BTNP after the surface coating, where the PEG layer can clearly be seen. The image of this PEG layer and the calculated spacing between individual PEG grafts suggest that the polymers are in a "brush" conformation, minimizing unwanted interactions with biologicals (such as protein adsorption on the surface) and providing superior stability.[32,44] The unmodified BTNPs are not soluble in water and form large aggregates as shown in the top panel of Figure 3C. However, the coating of the nanoparticles with PEG yields stable dispersions of BTNPs in water and physiological media. This claim is supported by the bottom TEM micrograph in Figure 3C, depicting well-dispersed BTNPs in the absence of large aggregates. To quantify the differences in solubility, we performed dynamic light scattering (DLS) measurements on unmodified nanoparticles compared to PEGylated BTNPs (the measurements are summarized in Table S3). The measured size of the unmodified BTNPs averaged 1837 nm with a standard deviation of 191 nm, confirming the presence of large aggregates and extremely poor stability of the solution. On the other hand, upon PEG stabilization, the size of the BTNPs averaged 309 nm with a standard deviation of 15.7 nm. Thus, we conclude that coating the BTNP surface with covalently bound hydrophilic PEG polymers succeeds in the preparation of stable nanoparticle dispersions for biomedical applications.

Exploiting Functionalized PEG to Create Fluorescent BTNPs and to Tune Surface Charge. Green fluorescent PEG is readily available, but many applications require the use of a different fluorophore due to the overlap of fluorescent spectra or the poor transmission of green light through tissue. We were able to create orange and red fluorescent nanoparticles using functionalized fluorescent molecules and BTNPs coated with bifunctionalized PEG, providing NH_2 or SH groups available for binding. The orange fluorescent nanoparticles were synthesized by attaching a maleimide-labeled cyanine3 to a thiolated BTNP surface. Synthesis of the red fluorescent nanoparticles took advantage of a cyanine5-NHS dye that was conjugated to amine groups on the PEG molecules on the nanoparticle surface. Through these methods, the BTNP fluorescence can be tuned to a specific application and will work with standard 488 nm/532 nm/633 nm fluorescent light sources (Figure 4A).

Surface charge is another variable that is relevant to optimizing the surface properties of nanoparticles for biomedical applications. For example, a study of polyethylenimine wrapping of BTNPs found that the positively charged polymers enhanced the interactions with cell membranes and increased cell uptake of the nanoparticles.[28] Conversely, it may be of interest to add more negatively charged molecules to minimize unwanted nonspecific attachment of the nanoparticles to cells not intended as a target. We utilized heterobifunctionalized silane-PEG-COOH to achieve more negative surface charge and silane-PEG-NH_2 to achieve more positive surface charge (Figure 4B). The effects were investigated by taking ζ-potential measurements of the nanoparticles dispersed in PBS with a pH of 7.4. The ζ-potential of unmodified BTNPs was measured to be -11 ± 1.1 mV. After PEG coating of the surface, the ζ-potential decreased to -16 ± 0.32 mV. Adding free COOH groups on the surface led to more negative charge; the ζ-potential was measured to be -19 ± 0.70 mV. Finally, adding NH_2 groups shifted the ζ-potential in the positive direction to values of -6.8 ± 0.46 mV. The ζ-potential difference between the unmodified and the PEGylated nanoparticles was found to be statistically significant with a p-value of 0.002 (based on a two-tailed Student's t test, $n = 3$). The null hypothesis was also rejected when comparing the means of the PEGylated nanoparticles vs the COOH-functionalized BTNPs, and the PEGylated nanoparticles vs the NH_2-functionalized BTNPs, with p-values of 0.001 and 0.00001, respectively.

These results demonstrate that we can alter the surface charge of the BTNPs; however, we can also tune how much the ζ-potential will shift. In the samples presented in Figure 4B, the charged bifunctional PEG was covering a 40% portion of the BTNP surface with the rest being monofunctionalized PEG

https://dx.doi.org/10.1021/acsanm.0c00019
ACS Appl. Nano Mater. XXXX, XXX, XXX−XXX

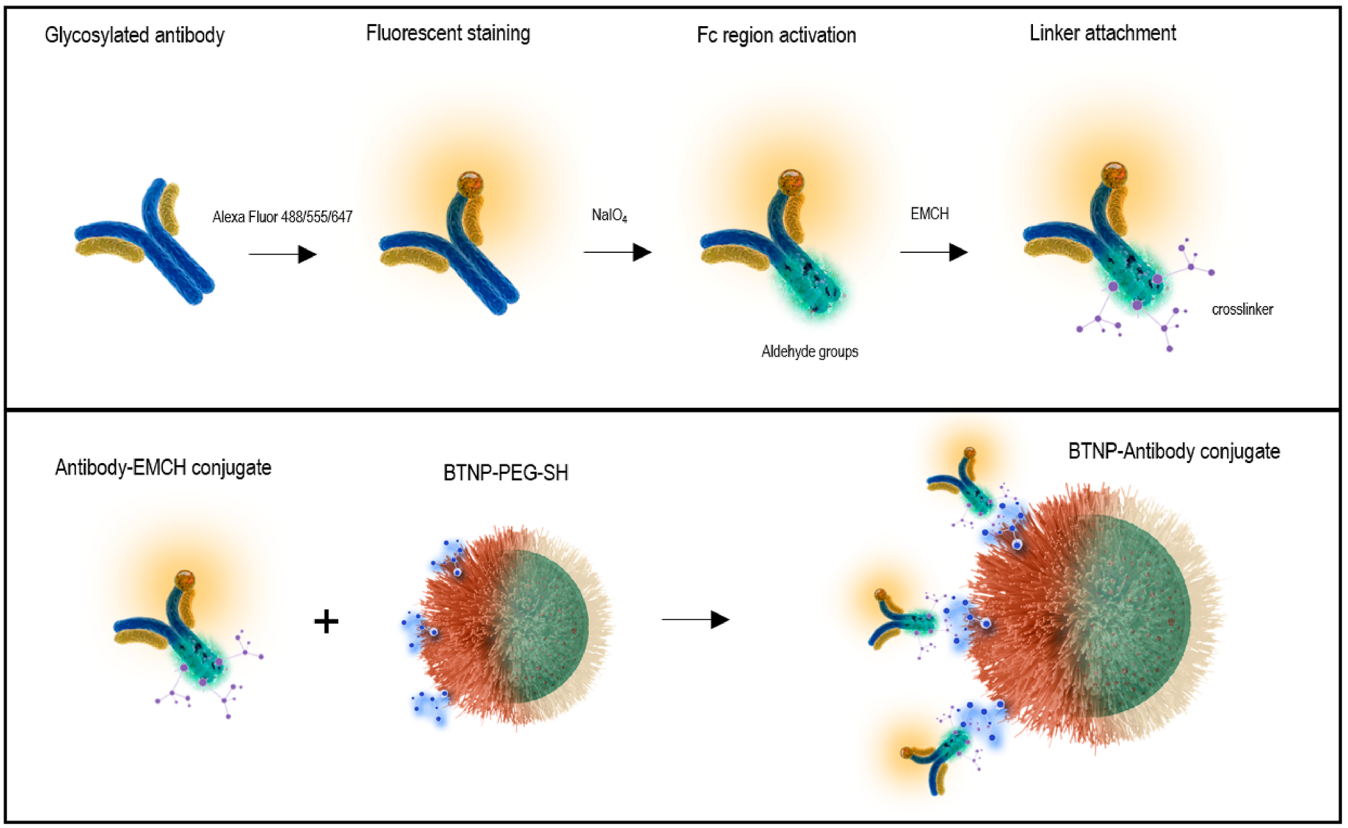

Figure 5. Schematic of our directional antibody conjugation chemistry. A glycosylated antibody is first fluorescently labeled, and then aldehyde groups are created on the Fc region. The hydrazide portion of an EMCH cross-linker binds to the aldehyde groups while the maleimide portion attaches to the thiolated BTNP surface.

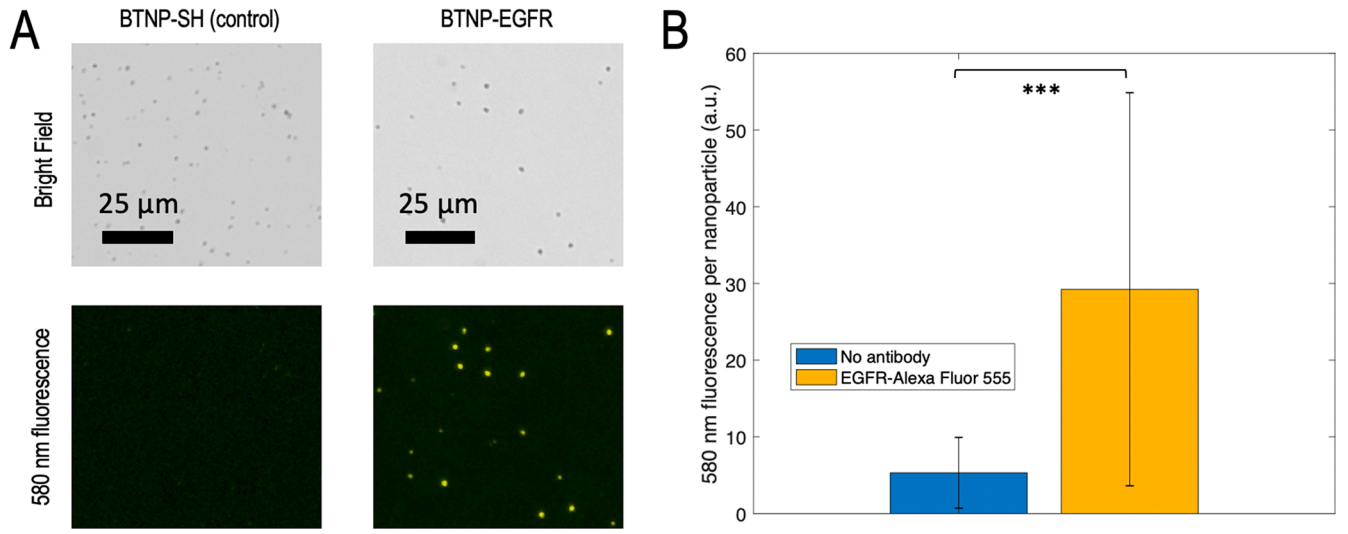

Figure 6. (A) Fluorescent micrographs of control BTNPs compared to BTNPs with conjugated fluorescent EGFR antibodies. The strong fluorescence confirms the presence of attached antibodies. (B) Quantitative analysis of fluorescence showed that the difference is statistically significant with p-value lower than 0.001 (n = 638).

with no charged groups. The ratio of charged biofunctionalized PEG to monofunctionalized PEG in the surface coating determines how much the ζ-potential is affected, as demonstrated in Figure 4C. In this experiment, we tested BTNPs with surface coatings containing 10%, 20%, or 50% of PEG-NH_2 compared to PEGylated BTNPs with no charged groups in the PEG layer. As apparent, increasing the proportion of PEG-NH_2 in the surface PEG layer correlates with increasing ζ-potential. Thus, through thoughtful composition of the PEG surface coating, we can tune the ζ-potential to fit our desired application.

Directional Conjugation of IgG Antibodies to the BTNP Surface. Our conjugation chemistry was developed and optimized on a monoclonal anti-EGFR antibody (clone 225), but it translates to any IgG antibody that is glycosylated (Figure 5). The anti-EGFR antibody was first stained with

https://dx.doi.org/10.1021/acsanm.0c00019
ACS Appl. Nano Mater. XXXX, XXX, XXX−XXX

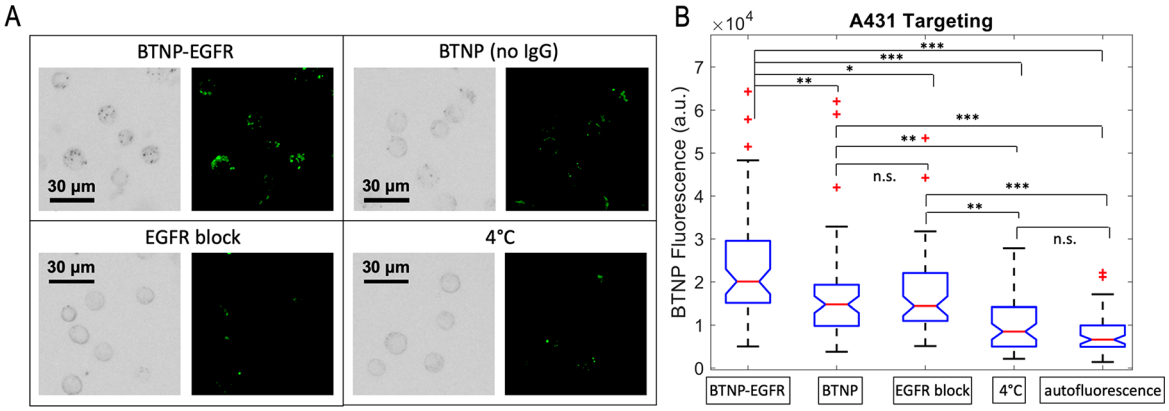

Figure 7. (A) Bright field and fluorescent images of A431 cells after a 2 h incubation with the BTNPs. Tested conditions included the targeted sample (BTNPs with conjugated antibodies), the nontargeted sample (BTNPs without antibodies), EGFR blocking with free-floating IgG, and targeted BTNP incubation at 4 °C. Both bright-field and fluorescence images show strong binding of the BTNPs in the targeted case while there is a significant decrease in the signal for the nontargeted sample and the EGFR blocking sample. Incubation at 4 °C yielded images indistinguishable from cell autofluorescence, suggesting minimal binding to cells. (B) Quantification of the BTNP binding through analysis of FITC fluorescence per cell. BTNP-EGFR binding was significantly stronger than all the other tested conditions (n.s. = not statistically significant, $*p < 0.05$, $**p < 0.01$, $***p < 0.001$, $n = 60$).

orange fluorescent Alexa Fluor 555 to enable the verification of successful binding to the BTNP surface. (Other fluorescent options such as Alexa Fluor 488 or 647 can be selected instead, depending on the application.) Reacting the antibody with sodium periodate then induced oxidation of the Fc region, yielding reactive aldehyde groups. The presence of aldehydes was confirmed with a Purpald test (qualitative results are shown in Figure S2). To covalently bind this modified antibody to the nanoparticle surface, we utilized a midlength (11.8 Å, MW 225.24) *N*-ε-maleimidocaproic acid hydrazide (EMCH) cross-linker. The hydrazide end of EMCH can efficiently react with aldehydes in amine-free buffers with pH of 6.5−7.5 to form hydrazone bonds and create a stable conjugate. The reaction resulted in antibodies with the maleimide ends of EMCH exposed on the Fc region. These maleimide groups then reacted with available thiol groups on the nanoparticle surface to form thioether bonds. Stable conjugates of the BTNPs and antibodies were created where the Fc region was bound to the BTNP surface and the antibody binding region was facing outward to increase the efficiency of molecular targeting.

The presence of antibodies on the BTNP surface was verified by fluorescent microscopy. Figure 6A shows control PEGylated nanoparticles without any antibodies exhibiting minimal orange autofluorescence. However, upon the conjugation of Alexa Fluor 555-labeled EGFR antibody, strong fluorescent signals are present. The fluorescence of $n = 638$ nanoparticles for both conditions was quantified. A two-tailed Student's t test revealed that the difference of the means was statistically significant with $p < 0.001$ (Figure 6B). In addition, we sought to quantify the amount of antibody that conjugated to the nanoparticle surface. Using a spectrofluorometer, we measured the fluorescent antibody concentration in the BTNP sample to average 4.59 ± 1.67 μg/mL. Using the antibody molecular weight and the number of nanoparticles in the sample, we were able to compute that the number of antibodies bound per nanoparticle averaged 55.5 ± 16.5. The calculation is shown in detail in Figure S3. On the basis of the fluorescent microscopy results and the spectrofluorometer data, we conclude that we can successfully conjugate anti-EGFR antibodies to BTNPs at quantities enabling molecular targeting of the BTNPs to cells of interest.

Molecular Targeting of BTNPs to A431 Cells. Next, we evaluated the molecular targeting capabilities with cultured cells. Human epidermoid carcinoma cells (A431 cell line), which highly overexpress EGFR, were incubated with the BTNP−antibody conjugates at 36 °C for 2 h. The 2 h time point was chosen based on studying cell uptake rates comparing the incubation of antibody-conjugated BTNPs and control BTNPs with the cells over time (the results are shown in Figure S6). The final concentration of the BTNPs in our sample was 50 μg/mL, which does not cause any decrease in cell viability as indicated by our studies (cytocompatibility data are included in Figure S5). Additionally, three control experiments were carried as part of this molecular targeting study. First, to assess the levels of nonspecific binding, PEGylated BTNPs without conjugated antibodies were incubated with the cells under the same conditions. Second, to study the role of EGFR in BTNP binding and uptake, we incubated the BTNP−antibody conjugates with the cells in the presence of free-floating anti-EGFR IgG to block the receptors and inhibit any EGFR-mediated effects. Third, to inhibit all endocytosis effects, we performed the incubation at 4 °C. The molecular targeting results were quantified by using fluorescent microscopy as all the BTNPs used were labeled with FITC for imaging purposes. After 2 h of incubation, the unbound nanoparticles were cleared by using a 5 μm centrifuge filter, and the cells were imaged with a fluorescent microscope.

BTNP−antibody conjugates were found to have high levels of binding to A431 cells. This is apparent from both bright field and fluorescent micrographs shown in Figure 7A. On the other hand, there was an evident decrease in the signal in the case of nontargeted BTNPs (without the antibody) and in the case of EGFR blocking (with the free-floating antibody). Finally, no visible BTNP binding was observed in the 4 °C condition as the signal was indistinguishable from cell autofluorescence. To quantify these results, we isolated regions of $n = 60$ cells from the bright field images and analyzed FITC emission in the corresponding regions in the fluorescent images. The mean fluorescence per cell in the targeted BTNP sample (with conjugated antibodies) was $2.42 \times 10^4 \pm 1.58 \times$

https://dx.doi.org/10.1021/acsanm.0c00019
ACS Appl. Nano Mater. XXXX, XXX, XXX−XXX

10^4 au. The control samples averaged $1.70 \times 10^4 \pm 1.09 \times 10^4$ au for the nontargeted condition (no antibodies), $1.79 \times 10^4 \pm 1.22 \times 10^4$ au for the EGFR blocking condition (free-floating IgG), and $1.03 \times 10^4 \pm 0.684 \times 10^4$ au for the 4 °C incubation. Furthermore, cell autofluorescence with no BTNPs was quantified as $0.796 \times 10^4 \pm 0.450 \times 10^4$ au per cell. The statistical significance was assessed by using the Mann−Whitney U-test since the data distributions are not normal (as confirmed by the Lilliefors test with resulting p-values smaller than 0.01 for all tested conditions). The targeted BTNP−antibody sample fluorescence increase was statistically significant compared to all conditions, with $p < 0.01$ compared to the nontargeted sample, $p < 0.05$ compared to the EGFR blocking sample, and $p < 0.001$ compared to 4 °C incubation and cell autofluorescence. The difference between the nontargeted sample and the EGFR blocking sample was found not statistically significant; however, both conditions had significantly stronger fluorescence than 4 °C and autofluorescence ($p < 0.01$ and $p < 0.001$, respectively). Finally, the fluorescence of the 4 °C incubation sample was not significantly different from cell autofluorescence. The statistically significant differences between the targeted and nontargeted samples were preserved when we analyzed a large number of cells using flow cytometry (described in Figure S4). On the basis of all presented evidence, we conclude that while there is some nonspecific binding of nontargeted BTNPs to the cells, the binding levels can be significantly increased by conjugating targeting antibodies to the BTNP surface. The BTNP−antibody conjugate binding to the cells is EGFR-mediated and reliant on the availability of the EGFR receptor.

CONCLUSIONS

In summary, we were able to prepare stable dispersions of BTNPs by covalently binding PEG polymers to the nanoparticle surface. The PEGylation chemistry enabled us to perform further modifications including fluorescent labeling, tuning of the surface charge, and directional conjugation of IgG antibodies for cell-specific targeting. These all are critical modifications of BTNPs that can expand the nanoparticle applications in medical imaging, cancer therapy, and neurostimulation. First, having a stable solution of BTNPs minimizes the negative effects linked to nanoparticle aggregation such as decreased cellular uptake or potential cytotoxicity. Furthermore, nanoparticle aggregation in vivo can decrease the nanoparticle circulation time, interfering with efficient delivery to target sites for imaging or therapy. Additionally, large nanoparticle clusters can prevent efforts to facilitate blood−brain barrier crossing for applications in the brain. Stable BTNP dispersion also improves the shelf life of the nanoparticles. Second, fluorescent labeling is of importance to confirming nanoparticle delivery to a target location or studying clearance mechanisms in vivo. Thanks to our multicolor fluorescent labeling, the nanoparticle excitation/emission wavelengths can be selected depending on the experimental setup, avoiding interference with other fluorescent agents that might be used simultaneously with the BTNPs. Third, tuning the surface charge directly impacts how the nanoparticles will interact with both biological and nonbiological samples. A charged surface can be utilized to facilitate or inhibit nanoparticle binding to a substrate. Similarly, positively charged nanoparticles can be endocytosed by cells at higher rates while negatively charged nanoparticles have less binding to membranes, minimizing unwanted nonspecific interactions. Last, antibody conjugation is critical for molecular targeting to specific cells of interest. BTNPs targeted to tumor cells can be used in a multifunctional fashion for both cancer imaging (through either SHG or fluorescence) and therapy (via photothermal therapy, drug or gene delivery, or noninvasive application of chronic ultrasound). Similarly, neuron stimulation applications can benefit from having the BTNPs targeted to different subpopulations of cells, such as excitatory neurons, inhibitory neurons, genetically transfected neurons, and so on. Overall, this versatile set of surface modifications enables seamless preparation of BTNPs with desirable properties for applications in imaging, therapy, or brain stimulation.

ASSOCIATED CONTENT

Supporting Information

The Supporting Information is available free of charge at https://pubs.acs.org/doi/10.1021/acsanm.0c00019.

List of materials and vendors with specific product numbers (Table S1); PEG reaction mixture reagents and amounts for different nanoparticle conditions (Table S2); comparison of solubility of unmodified and PEGylated nanoparticles as measured by dynamic light scattering (Table S3); quantification of PEG polymers bound to the BTNP surface (Figure S1); Purpald test confirming presence of aldehydes (Figure S2); quantification of IgG conjugated to the BTNP surface (Figure S3); flow cytometry characterization of BTNP and BTNP−EGFR uptake (Figure S4); cytocompatibility evaluation of the BTNPs incubated with A431 cells (Figure S5); rates of BTNP and BTNP−antibody binding to A431 cells over time (Figure S6) (PDF)

AUTHOR INFORMATION

Corresponding Author

Geoffrey P. Luke − *Thayer School of Engineering, Dartmouth College, Hanover, New Hampshire 03755, United States; Translational Engineering in Cancer Research Program, Norris Cotton Cancer Center, Lebanon, New Hampshire 03766, United States*; Email: geoffrey.p.luke@dartmouth.edu

Authors

Tomas Jordan − *Thayer School of Engineering, Dartmouth College, Hanover, New Hampshire 03755, United States;* orcid.org/0000-0002-7432-1929

Mikaela A. O'Brien − *Thayer School of Engineering, Dartmouth College, Hanover, New Hampshire 03755, United States*

Catalina-Paula Spatarelu − *Thayer School of Engineering, Dartmouth College, Hanover, New Hampshire 03755, United States*

Complete contact information is available at: https://pubs.acs.org/10.1021/acsanm.0c00019

Notes

The authors declare no competing financial interest.

ACKNOWLEDGMENTS

This work was supported by National Institutes of Health Grant R21EY029422.

■ ABBREVIATIONS

BTNPs, barium titanate nanoparticles; PEG, poly(ethylene glycol); CD, cyclodextrin; PBS, phosphate buffered saline; TEM, transmission electron microscopy; PFM, piezoresponse force microscopy; FTIR, Fourier-transform infrared spectroscopy; ATR, attenuated total reflectance; DLS, dynamic light scattering; EGFR, epidermal growth factor receptor; EMCH, *N*-ε-maleimidocaproic acid hydrazide; XRD, X-ray powder diffraction.

■ REFERENCES

(1) Vijatovic, M. M.; Bobic, J. D.; Stojanovic, B. D. History and Challenges of Barium Titanate: Part I. *Sci. Sinter.* **2008**, *40*, 155−165.

(2) Bansal, V.; Poddar, P.; Ahmad, A.; Sastry, M. Room-Temperature Biosynthesis of Ferroelectric Barium Titanate Nanoparticles. *J. Am. Chem. Soc.* **2006**, *128*, 11958−11963.

(3) Shaw, T. M.; Trolier-McKinstry, S.; McIntyre, P. C. The Properties of Ferroelectric Films at Small Dimensions. *Annu. Rev. Mater. Sci.* **2000**, *30*, 263−298.

(4) Pantazis, P.; Maloney, J.; Wu, D.; Fraser, S. E. Second Harmonic Generating (SHG) Nanoprobes for in Vivo Imaging. *Proc. Natl. Acad. Sci. U. S. A.* **2010**, *107*, 14535−14540.

(5) Ciofani, G.; Danti, S.; D'Alessandro, D.; Moscato, S.; Petrini, M.; Menciassi, A. Barium Titanate Nanoparticles: Highly Cytocompatible Dispersions in Glycol-Chitosan and Doxorubicin Complexes for Cancer Therapy. *Nanoscale Res. Lett.* **2010**, *5*, 1093−1101.

(6) Nacer, R. S.; Silva, B. A. K. da; Poppi, R. R.; Silva, D. K. M.; Cardoso, V. S.; Delben, J. R. J.; Delben, A. A. S. T. Biocompatibility and Osteogenesis of the Castor Bean Polymer Doped with Silica (SiO_2) or Barium Titanate (BaTiO3) Nanoparticles. *Acta Cir. Bras.* **2015**, *30*, 255−263.

(7) Singh, K. C.; Nath, A. K. Barium Titanate Nanoparticles Produced by Planetary Ball Milling and Piezoelectric Properties of Corresponding Ceramics. *Mater. Lett.* **2011**, *65*, 970−973.

(8) Rajabi, A. H.; Jaffe, M.; Arinzeh, T. L. Piezoelectric Materials for Tissue Regeneration: A Review. *Acta Biomater.* **2015**, *24*, 12−23.

(9) Jianqing, F.; Huipin, Y.; Xingdong, Z. Promotion of osteogenesis by a piezoelectric biological ceramic. *Biomaterials* **1997**, *18*, 1531−1534.

(10) Ciofani, G.; Rocca, A.; Marino, A.; Rocca, V.; Moscato, S.; de Vito, G.; Piazza, V.; Mazzolai, B.; Mattoli, V.; Ngo-Anh, T. J. Barium Titanate Nanoparticles and Hypergravity Stimulation Improve Differentiation of Mesenchymal Stem Cells into Osteoblasts. *Int. J. Nanomed.* **2015**, 433.

(11) Marino, A.; Arai, S.; Hou, Y.; Sinibaldi, E.; Pellegrino, M.; Chang, Y.-T.; Mazzolai, B.; Mattoli, V.; Suzuki, M.; Ciofani, G. Piezoelectric Nanoparticle-Assisted Wireless Neuronal Stimulation. *ACS Nano* **2015**, *9*, 7678−7689.

(12) Rojas, C.; Tedesco, M.; Massobrio, P.; Marino, A.; Ciofani, G.; Martinoia, S.; Raiteri, R. Acoustic Stimulation Can Induce a Selective Neural Network Response Mediated by Piezoelectric Nanoparticles. *J. Neural Eng.* **2018**, *15*, 036016.

(13) Marino, A.; Battaglini, M.; De Pasquale, D.; Degl'Innocenti, A.; Ciofani, G. Ultrasound-Activated Piezoelectric Nanoparticles Inhibit Proliferation of Breast Cancer Cells. *Sci. Rep.* **2018**, *8*, 6257.

(14) Marino, A.; Almici, E.; Migliorin, S.; Tapeinos, C.; Battaglini, M.; Cappello, V.; Marchetti, M.; de Vito, G.; Cicchi, R.; Pavone, F. S.; Ciofani, G. Piezoelectric Barium Titanate Nanostimulators for the Treatment of Glioblastoma Multiforme. *J. Colloid Interface Sci.* **2019**, *538*, 449−461.

(15) Genchi, G. G.; Marino, A.; Rocca, A.; Mattoli, V.; Ciofani, G. Barium Titanate Nanoparticles: Promising Multitasking Vectors in Nanomedicine. *Nanotechnology* **2016**, *27*, 232001.

(16) Dempsey, W. P.; Fraser, S. E.; Pantazis, P. SHG Nanoprobes: Advancing Harmonic Imaging in Biology. *BioEssays* **2012**, *34*, 351−360.

(17) Čulić-Viskota, J.; Dempsey, W. P.; Fraser, S. E.; Pantazis, P. Surface Functionalization of Barium Titanate SHG Nanoprobes for in Vivo Imaging in Zebrafish. *Nat. Protoc.* **2012**, *7*, 1618−1633.

(18) Grange, R.; Lanvin, T.; Hsieh, C.-L.; Pu, Y.; Psaltis, D. Imaging with Second-Harmonic Radiation Probes in Living Tissue. *Biomed. Opt. Express* **2011**, *2*, 2532.

(19) Liu, J.; Cho, I.-H.; Cui, Y.; Irudayaraj, J. Second Harmonic Super-Resolution Microscopy for Quantification of MRNA at Single Copy Sensitivity. *ACS Nano* **2014**, *8*, 12418−12427.

(20) Hsieh, C.-L.; Grange, R.; Pu, Y.; Psaltis, D. Three-Dimensional Harmonic Holographic Microcopy Using Nanoparticles as Probes for Cell Imaging. *Opt. Express* **2009**, *17*, 2880.

(21) Chandler, C. D.; Roger, C.; Hampden-Smith, M. J. Chemical Aspects of Solution Routes to Perovskite-Phase Mixed-Metal Oxides from Metal-Organic Precursors. *Chem. Rev.* **1993**, *93*, 1205−1241.

(22) Hernandez, B. A.; Chang, K.-S.; Fisher, E. R.; Dorhout, P. K. Sol−Gel Template Synthesis and Characterization of $BaTiO_3$ and $PbTiO_3$ Nanotubes. *Chem. Mater.* **2002**, *14*, 480−482.

(23) Kwon, S.-G.; Park, B.-H.; Choi, K.; Choi, E.-S.; Nam, S.; Kim, J.-W.; Kim, J.-H. Solvothermally Synthesized Tetragonal Barium Titanate Powders Using H_2O/EtOH Solvent. *J. Eur. Ceram. Soc.* **2006**, *26*, 1401−1404.

(24) Xu, H.; Gao, L.; Guo, J. Preparation and Characterizations of Tetragonal Barium Titanate Powders by Hydrothermal Method. *J. Eur. Ceram. Soc.* **2002**, *22*, 1163−1170.

(25) Brutchey, R. L.; Morse, D. E. Template-Free, Low-Temperature Synthesis of Crystalline Barium Titanate Nanoparticles under Bio-Inspired Conditions. *Angew. Chem., Int. Ed.* **2006**, *45*, 6564−6566.

(26) Blanco-Lopez, M. C.; Rand, B.; Riley, F. L. The Properties of Aqueous Phase Suspensions of Barium Titanate. *J. Eur. Ceram. Soc.* **1997**, *17*, 281−287.

(27) Ciofani, G.; Danti, S.; Moscato, S.; Albertazzi, L.; D'Alessandro, D.; Dinucci, D.; Chiellini, F.; Petrini, M.; Menciassi, A. Preparation of Stable Dispersion of Barium Titanate Nanoparticles: Potential Applications in Biomedicine. *Colloids Surf., B* **2010**, *76*, 535−543.

(28) Dempsey, C.; Lee, I.; Cowan, K. R.; Suh, J. Coating Barium Titanate Nanoparticles with Polyethylenimine Improves Cellular Uptake and Allows for Coupled Imaging and Gene Delivery. *Colloids Surf., B* **2013**, *112*, 108−112.

(29) Serra-Gómez, R.; Martinez-Tarifa, J. M.; González-Benito, J.; González-Gaitano, G. Cyclodextrin-Grafted Barium Titanate Nanoparticles for Improved Dispersion and Stabilization in Water-Based Systems. *J. Nanopart. Res.* **2016**, *18*, 24.

(30) Wang, M.; Thanou, M. Targeting Nanoparticles to Cancer. *Pharmacol. Res.* **2010**, *62*, 90−99.

(31) Hsieh, C.-L.; Grange, R.; Pu, Y.; Psaltis, D. Bioconjugation of Barium Titanate Nanocrystals with Immunoglobulin G Antibody for Second Harmonic Radiation Imaging Probes. *Biomaterials* **2010**, *31*, 2272−2277.

(32) Jokerst, J. V.; Lobovkina, T.; Zare, R. N.; Gambhir, S. S. Nanoparticle PEGylation for Imaging and Therapy. *Nanomedicine* **2011**, *6*, 715−728.

(33) Suk, J. S.; Xu, Q.; Kim, N.; Hanes, J.; Ensign, L. M. PEGylation as a Strategy for Improving Nanoparticle-Based Drug and Gene Delivery. *Adv. Drug Delivery Rev.* **2016**, *99*, 28−51.

(34) Chang, S.-J.; Liao, W.-S.; Ciou, C.-J.; Lee, J.-T.; Li, C.-C. An Efficient Approach to Derive Hydroxyl Groups on the Surface of Barium Titanate Nanoparticles to Improve Its Chemical Modification Ability. *J. Colloid Interface Sci.* **2009**, *329*, 300−305.

(35) Francis, R.; Joy, N.; Aparna, E. P.; Vijayan, R. Polymer Grafted Inorganic Nanoparticles, Preparation, Properties, and Applications: A Review. *Polym. Rev.* **2014**, *54*, 268−347.

(36) Kumar, S.; Aaron, J.; Sokolov, K. Directional Conjugation of Antibodies to Nanoparticles for Synthesis of Multiplexed Optical Contrast Agents with Both Delivery and Targeting Moieties. *Nat. Protoc.* **2008**, *3*, 314−320.

(37) Homan, K. A.; Souza, M.; Truby, R.; Luke, G. P.; Green, C.; Vreeland, E.; Emelianov, S. Silver Nanoplate Contrast Agents for *in Vivo* Molecular Photoacoustic Imaging. *ACS Nano* **2012**, *6*, 641−650.

https://dx.doi.org/10.1021/acsanm.0c00019
ACS Appl. Nano Mater. XXXX, XXX, XXX−XXX

(38) Yamamoto, T.; Urabe, K.; Banno, H. BaTiO $_3$ Particle-Size Dependence of Ferroelectricity in BaTiO $_3$ /Polymer Composites. *Jpn. J. Appl. Phys.* **1993**, *32*, 4272−4276.
(39) Hiroki, A.; LaVerne, J. A. Decomposition of Hydrogen Peroxide at Water−Ceramic Oxide Interfaces. *J. Phys. Chem. B* **2005**, *109*, 3364−3370.
(40) Giamello, E.; Calosso, L.; Fubini, B.; Geobaldo, F. Evidence of Stable Hydroxyl Radicals and Other Oxygen Radical Species Generated by Interaction of Hydrogen Peroxide with Magnesium Oxide. *J. Phys. Chem.* **1993**, *97*, 5735−5740.
(41) HARWOOD, M. G.; POPPER, P.; RUSHMAN, D. F. Curie Point of Barium Titanate. *Nature* **1947**, *160*, 58−59.
(42) Shen, Y.; Wu, P. Two-Dimensional ATR−FTIR Spectroscopic Investigation on Water Diffusion in Polypropylene Film: Water Bending Vibration. *J. Phys. Chem. B* **2003**, *107*, 4224−4226.
(43) Li, C.-C.; Chang, S.-J.; Lee, J.-T.; Liao, W.-S. Efficient Hydroxylation of BaTiO3 Nanoparticles by Using Hydrogen Peroxide. *Colloids Surf., A* **2010**, *361*, 143−149.
(44) Perry, J. L.; Reuter, K. G.; Kai, M. P.; Herlihy, K. P.; Jones, S. W.; Luft, J. C.; Napier, M.; Bear, J. E.; DeSimone, J. M. PEGylated PRINT Nanoparticles: The Impact of PEG Density on Protein Binding, Macrophage Association, Biodistribution, and Pharmacokinetics. *Nano Lett.* **2012**, *12*, 5304−5310.

https://dx.doi.org/10.1021/acsanm.0c00019
ACS Appl. Nano Mater. XXXX, XXX, XXX−XXX